Grafting of Single, Stimuli-Responsive Poly(ferrocenylsilane) Polymer Chains to Gold Surfaces

Shan Zou, Yujie Ma,† Mark A. Hempenius, Holger Schönherr, and G. Julius Vancso*

Materials Science and Technology of Polymers, MESA+ Institute for Nanotechnology and Faculty of Science and Technology, University of Twente, 7500 AE Enschede, The Netherlands

Received December 11, 2003. In Final Form: May 10, 2004

Redox-responsive poly(ferrocenylsilane) (PFS) polymer molecules were attached individually to gold surfaces for force spectroscopy experiments on the single molecule level. By grafting ethylenesulfide-functionalized PFS into the defects of preformed self-assembled monolayers (SAMs) of different ω-mercaptoalkanols on Au(111), the surface coverage of PFS macromolecules could be conveniently controlled. Atomic force microscopy (AFM), contact angle, as well as cyclic and differential pulse voltammetry measurements were carried out to characterize the morphology, wettability, and surface coverage of the grafted layers. The values of the PFS surface coverage were found to depend on the chain length of the ω-mercaptoalkanol molecules and on the concentration of the PFS solution but not on the insertion time or on the molar mass of PFS. The equilibrium surface coverages were successfully described by Langmuir adsorption isotherms. For low-surface coverage values ($<6.2 \times 10^{-4}$ chain/nm^2), achieved by PFS insertion from very dilute solutions (8×10^{-6} M) into long-chain SAMs, AFM and differential pulse voltammetry showed that surfaces exposing isolated individual polymer chains were obtained. The isolated PFS macromolecules were subjected to in situ AFM-based single molecule force spectroscopy (SMFS) measurements. The single chain elasticity of PFS in isopropanol (and ethanol) was fitted with the modified freely jointed chain (m-FJC) model. This procedure yielded a Kuhn segment length of 0.33 ± 0.05 nm and a segment elasticity of 32 ± 5 nN/nm.

Introduction

The construction of artificial molecular machines, in which molecules mechanically work as machines and motors powered by external energy sources in a controllable manner, has recently attracted a great deal of attention.[1−4] Nanomechanical devices or molecular machines will, for a broad range of applications, most likely be powered by light or other kinds of electromagnetic radiation.[5] Complementary to the artificial machines, there exists a plethora of natural ones, such as flagellae, which drive the motions of bacteria,[6] or ATP synthase, a rotary motor responsible for the synthesis of ATP from ADP.[7] The potential of light-powered molecular machines has been explored, among others, by the groups of Gaub,[5] Brouwer,[8] and Feringa.[2−4]

The molecular devices explored by now all fit the typical behavior of "machines". Macroscopic electromechanical actuators have been proposed a decade ago[9] and have been pioneered in many different laboratories,[10−12] yet true molecular machines powered by a redox process are still largely unknown. One of the key challenges is to interface such nanometer-sized or molecular devices with the macroscopic world.[5] The detection, spectroscopy, and identification of single molecules are therefore essential elements for a successful construction of molecular machines.

Atomic force microscopy (AFM),[13] enabling both visualization of single molecules[14] and determination of properties for single chains,[15] became a versatile method for the study and characterization of polymeric materials down to the nanometer scale. By providing nanometer scale spatial resolution and piconewton range force sensitivity combined with the possibility to in situ monitor molecular conformations down to milliseconds time scales, it is possible to determine intrinsic properties of single polymers and drive out such statistical factors as molecular

* Corresponding author. E-mail: g.j.vancso@utwente.nl.
† Current address: College of Chemistry and Chemical Technology, Shanghai Jiao Tong University, Shanghai 200240, China.

(1) Stoddart, J. F. *Acc. Chem. Res.* **2001**, *34*, 410.
(2) Hania, P. R.; Telesca, R.; Lucas, L. N.; Pugzlys, A.; van Esch, J.; Feringa, B. L.; Snijders, J. G.; Duppen, K. *J. Phys. Chem. A* **2002**, *106*, 8498.
(3) Geertsema, E. M.; Koumura, N.; ter Wiel, M. K. J.; Meetsma, A.; Feringa, B. L. *Chem. Commun.* **2002**, 2962.
(4) van Delden, R. A.; Hurenkamp, J. H.; Feringa, B. L. *Chem. Eur. J.* **2003**, *9*, 2845.
(5) Hugel, T.; Holland, N. B.; Cattani, A.; Moroder, L.; Seitz, M.; Gaub, H. E. *Science* **2002**, *296*, 1103.
(6) Samatey, F. A.; Imada, K.; Nagashima, S.; Vonderviszt, F.; Kumasaka, T.; Yamamoto, M.; Namba, K. *Nature* **2001**, *410*, 331.
(7) Noji, H.; Yasuda, R.; Yoshida, M.; Kinosita, K. *Nature* **1997**, *386*, 299.
(8) (a) Brouwer, A. M.; Frochot, C.; Gatti, F. G.; Leigh, D. A.; Mottier, L.; Paolucci, F.; Roffia, S.; Wurpel, G. W. H. *Science* **2001**, *291*, 2124. (b) Gatti, F. G.; León, S.; Wong, J. K. Y.; Bottari, G.; Altieri, A.; Morales, M. A. F.; Teat, S. J.; Frochot, C.; Leigh, D. A.; Brouwer, A. M.; Zerbetto, F. *P. Natl. Acad. Sci.* **2003**, *100*, 10.
(9) Baughman, R. H. *Synth. Met.* **1996**, *78*, 339.
(10) Smela, E.; Inganäs, O.; Lundström, I. *Science* **1995**, *268*, 1735.
(11) Kaneto, K.; Kaneko, M.; Min, Y.; MacDiarmid, A. G. *Synth. Met.* **1995**, *71*, 2211.
(12) Baughman, R. H.; Cui, C.; Zakhidov, A. A.; Iqbal, Z.; Barisci, J. N.; Spinks, G. M.; Wallace, G. G.; Mazzoldi, A.; De Rossi, D.; Rinzler, A. G.; Jaschinski, O.; Roth, S.; Kertesz, M. *Science* **1999**, *284*, 1340.
(13) Binnig, G.; Quate, C. F.; Gerber, C. *Phys. Rev. Lett.* **1986**, *56*, 930.
(14) (a) Hansma, H. G.; Vesenka, J.; Siegerist, C.; Kelderman, G.; Morrett, H.; Sinsheimer, R. L.; Elings, V.; Bustamante, C.; Hansma, P. K. *Science* **1992**, *256*, 1180. (b) Kumaki, J.; Nishikawa, Y.; Hashimoto, T. *J. Am. Chem. Soc.* **1996**, *118*, 3321. (c) Sheiko, S. S. *Adv. Polym. Sci* **1999**, *151*, 61. (d) Han, W. H.; Lindsay, S. M.; Dlakic, M.; Harington, R. E. *Nature* **1997**, *386*, 563. (e) Anselmetti, D.; Fritz, J.; Smith, B.; Fernandez-Busquets, X. *Single Mol.* **2000**, *1*, 53.
(15) (a) Leuba, S. H.; Zlatanova, J.; Karymov, M. A.; Bash, R.; Liu, Y.-Z.; Lohr, D.; Harrington, R. E.; Lindsay, S. M. *Single Mol.* **2000**, *1*, 185. (b) De Paris, R.; Strunz, T.; Oroszlan, K.; Güntherodt, H.-J.; Hegner, M. *Single Mol.* **2000**, *1*, 285. (c) Yamamoto, S.; Tsujii, Y.; Fukuda, T. *Macromolecules* **2000**, *33*, 5995. (d) Ortiz, C.; Hadziioannou, G. *Macromolecules* **1999**, *32*, 780. (e) Furukawa, K.; Ebata, K.; Matsumoto, N. *Appl. Phys. Lett.* **1999**, *75*, 781.

10.1021/la036341i CCC: $27.50
Published on Web 06/25/2004

mass distribution, diverse morphologies, and interchain interactions. Using AFM-based single molecule force spectroscopy, typical force fingerprints, elastic properties, and deformation of typical organic polymer materials, as well as bio-macromolecules, can also be revealed.[16,17] Recently, the elasticity changes induced by a cis−trans isomerization of an azobenzene-containing polymer have been reported.[5] Here we will utilize the unique combination of both the visualization and force sensing capabilities of AFM to address, that is, to locate, physically contact, and finally stretch, individual stimuli responsive macromolecules in an attempt to realize a single molecule machine.

The functionality of traditional organic polymers can be significantly enriched or complemented, and the corresponding scope can be enhanced through the development of the corresponding macromolecular chemistry of *inorganic and organometallic* materials. These polymers are of growing importance in light of the promising electrical, magnetic, optical, and catalytic properties that these materials possess.[18] In many cases these polymers possess important properties, which are distinctively different compared to those of their organic counterparts, owing to the presence of the incorporated "new" elements. For example, poly(ferrocenylsilanes) (PFSs),[19] composed of alternating ferrocene and alkylsilane units in the main chain, belong to this class of materials. In contrast to multistep procedures,[20] PFS can be employed, for instance, in single step reactive ion etching processes, due to the remarkable etching barrier properties of this organometallic polymer. As an example of the rich range of possible applications, thin films of block copolymers containing PFS blocks and various laterally structured surfaces comprising PFS have been used in "maskless" lithography applications as versatile templates.[21]

PFS can also be reversibly oxidized and reduced by means of electrochemistry.[22] In previous studies, the introduction of a thiol end functionality was exploited for the immobilization of poly(ferrocenylsilanes) on gold surfaces by self-assembly. Reversible redox-induced morphology and volume/thickness changes of neat self-assembled poly(ferrocenylsilane) monolayers on gold were studied in situ by using electrochemical atomic force microscopy (ECAFM), surface plasmon resonance spectroscopy (SPR), and X-ray reflectometry combined with cyclic and differential pulse voltammetry.[23,24] These effects are intimately related to the changes in solubility and conformation of the macromolecules upon oxidation or reduction, respectively. Thus, the surface-immobilized PFSs constitute an interesting electrochemically addressable stimulus-responsive system. The results obtained by differential pulse voltammetry (DPV)[25] also showed that the polymer chains in the PFS full layer were packed such that substantial interchain (through space) segment−segment interactions were observed.[23b]

To study the behavior, in particular the response to external redox or chemical stimuli, of PFS macromolecules on the single molecule level using AFM, surfaces that expose individual PFS macromolecules with large intermolecular spacings must be prepared. For this purpose, we utilized a generic strategy for isolation of PFS in self-assembled monolayers (SAMs).[26−29] The strategy relies on the insertion of thiol end-functionalized molecules into the defects formed in preformed SAMs when these are immersed in solvents.[30] The mechanism for this process consists of rapid dissociation of surface-bound thiols, possibly as disulfides, followed by slow macromolecule adsorption.[29b]

In this paper we report on the systematic investigation of the insertion behavior of ethylenesulfide-functionalized PFS into the defects of preformed SAMs (see Scheme 1) of different ω-mercaptoalkanols on Au(111). By a variation of the insertion time, the concentration of the PFS solution, the molecular mass of PFS, and the chain length of the ω-mercaptoalkanols, we determined the optimal conditions to obtain molecularly isolated PFS molecules. These isolated PFS macromolecules were then subjected to in situ stretching in AFM-based force spectroscopy experiments. These data form the basis for the investigation of the response of PFS macromolecules to external redox or chemical stimuli on the single molecule level.

(16) (a) Lee, G. U.; Chrisey, L. A.; Colton, R. J. *Science* **1994**, *266*, 771. (b) Rief, M.; Gautel, M.; Oesterhelt, F.; Fernandez, J.; Gaub, H. E. *Science* **1997**, *275*, 1295. (c) Marszalek, P. E.; Oberhauser, A. F.; Pang, Y. P.; Fernandez, J. M. *Nature* **1998**, *396*, 661. (d) Bemis, J. E.; Akhremitchev, B. B.; Walker, G. C. *Langmuir* **1999**, *15*, 2799. (e) Li, H. B.; Linke, W. A.; Oberhauser, A. F.; Carrion-Vazquez, M.; Kerkvliet, J. G.; Lu, H.; Marszalek, P. E.; Fernandez, J. M. *Nature* **2002**, *418*, 998. (f) Zhang, W.; Zhang, X. *Prog. Polym. Sci.* **2003**, *28*, 1271.

(17) For recent reviews see: (a) Janshoff, A.; Neitzert, M.; Oberdörfer, Y.; Fuchs, H. *Angew. Chem., Int. Ed.* **2000**, *39*, 3212. (b) Hugel, T.; Seitz, M. *Macromol. Rapid Commun.* **2001**, *22*, 989.

(18) (a) Abd-El-Aziz, A. S. *Macromol. Rapid Commun.* **2002**, *23*, 995. (b) Manners, I. *J. Polym. Sci., Part A: Polym. Chem.* **2002**, *40*, 179.

(19) (a) Kulbaba, K.; Manners, I. *Macromol. Rapid. Commun.* **2001**, *22*, 711. (b) Foucher, D. A.; Ziembinski, R.; Tang, B. Z.; Macdonald, P. M.; Massey, J.; Jaeger, C. R.; Vancso, G. J.; Manners, I. *Macromolecules* **1993**, *26*, 2878. (c) Nguyen, M. T.; Diaz, A. F.; Dement'ev, V. V.; Pannell, K. H. *Chem. Mater.* **1993**, *5*, 1389. (d) Pudelski, J. K.; Foucher, D. A.; Honeyman, C. H.; Macdonald, P. M.; Manners, I.; Barlow, S.; O'Hare, D. *Macromolecules* **1996**, *29*, 1894.

(20) (a) Spatz, J. P.; Sheiko, S.; Möller, M. *Adv. Mater.* **1996**, *8*, 513. (b) Park, M.; Harrison, C.; Chaikin, P. M.; Register, R. A.; Adamson, D. H. *Science* **1997**, *276*, 1401.

(21) (a) Lammertink, R. G. H.; Hempenius, M. A.; van den Enk, J. E.; Chan, V. Z.-H.; Thomas, E. L.; Vancso, G. J. *Adv. Mater.* **2000**, *12*, 98. (b) Lammertink, R. G. H.; Hempenius, M. A.; Vancso, G. J. *Chem. Mater.* **2001**, *13*, 429. (c) Cheng, J. Y.; Ross, C. A.; Lammertink, R. G. H.; Chan, V. Z. H.; Thomas, E. L.; Vancso, G. J. *Adv. Mater.* **2001**, *13*, 1174.

(22) Péter, M.; Lammertink, R. G. H.; Hempenius, M. A.; van Os, M.; Beulen, M. W. J.; Reinhoudt, D. N.; Knoll, W.; Vancso, G. J. *Chem. Commun.* **1999**, 359.

(23) (a) Péter, M.; Hempenius, M. A.; Lammertink, R. G. H.; Vancso, G. J. *Macromol. Symp.* **2001**, *167*, 285. (b) Péter, M.; Hempenius, M. A.; Kooij, E. S.; Jenkins, T. A.; Roser, S. J.; Knoll, W.; Vancso, G. J. *Langmuir* **2004**, *20*, 891. (c) Lammertink, R. G. H. Poly(ferrocenyldimethylsilanes) at the Interface of Chemistry and Materials Science: Synthesis, Structure-Properties and Thin Film Applications. Ph.D. Thesis, University of Twente, 2000.

(24) (a) Guo, W.; Jennings, G. K. *Langmuir* **2002**, *18*, 3123. (b) Guo, W. F.; Jennings, G. K. *Adv. Mater.* **2003**, *15*, 588.

(25) Kaifer, A. E.; Gomez-Kaifer, M. *Supramolecular Electrochemistry*; Wiley-VCH: Weinheim, 1999.

(26) Furukawa, K. *Acc. Chem. Res.* **2003**, *36*, 102.

(27) (a) Ulman, A. *An Introduction to Ultrathin Organic Films: From Langmuir−Blodgett to Self-Assembly*; Academic Press: New York, 1991; p 278. (b) Schreiber, F. *Prog. Surf. Sci.* **2000**, *65*, 151. (c) Dubois, L. H.; Nuzzo, R. G. *Annu. Rev. Phys. Chem.* **1992**, *43*, 437. (d) Poirier, G. E. *Chem. Rev.* **1997**, *97*, 1117.

(28) (a) Tour, J. M.; Jones, L.; Pearson, D. L.; Lamba, J. J. S.; Burgin, T. P.; Whitesides, G. M.; Allara, D. L.; Parikh, A. N.; Atre, S. *J. Am. Chem. Soc.* **1995**, *117*, 9529. (b) Bumm, L. A.; Arnold, J. J.; Cygan, M. T.; Dunbar, T. D.; Burgin, T. P.; Jones, L.; Allara, D. L.; Tour, J. M.; Weiss, P. S. *Science* **1996**, *271*, 1705.

(29) (a) Huisman, B.-H.; Schönherr, H.; Huck, W. T. S.; Friggeri, A.; van Manen, H.-J.; Menozzi, E.; Vancso, G. J.; van Veggel, F. C. J. M.; Reinhoudt, D. N. *Angew. Chem., Int. Ed.* **1999**, *38*, 2248. (b) Friggeri, A.; Schönherr, H.; van Manen, H.-J.; Huisman, B.; Vancso, G. J.; Huskens, J.; van Veggel, F. C. J. M.; Reinhoudt, D. N. *Langmuir* **2000**, *16*, 7757.

(30) (a) Schönenberger, C.; Sondag-Huethorst, J. A. M.; Jorritsma, J.; Fokkink, L. G. J. *Langmuir* **1994**, *10*, 611. (b) Sondag-Huethorst, J. A. M.; Schönenberger, C.; Fokkink, L. G. J. *J. Phys. Chem.* **1994**, *98*, 6826. (c) Nuzzo, R. G.; Allara, D. L. *J. Am. Chem. Soc.* **1983**, *105*, 4481. (d) Porter, M. D.; Bright, T. B.; Allara, D. L.; Chidsey, C. E. D. *J. Am. Chem. Soc.* **1987**, *109*, 3559. (e) Laibinis, P. E.; Fox, M. A.; Folkers, J. P.; Whitesides, G. M. *Langmuir* **1991**, *7*, 3167. (f) Vaidya, B.; Chen, J.; Porter, M. D.; Angelici, R. J. *Langmuir* **2001**, *17*, 6569.

Scheme 1. Schematic of Insertion Strategy Employed To Immobilize Isolated PFS Macromolecules on Gold Surfaces[a]

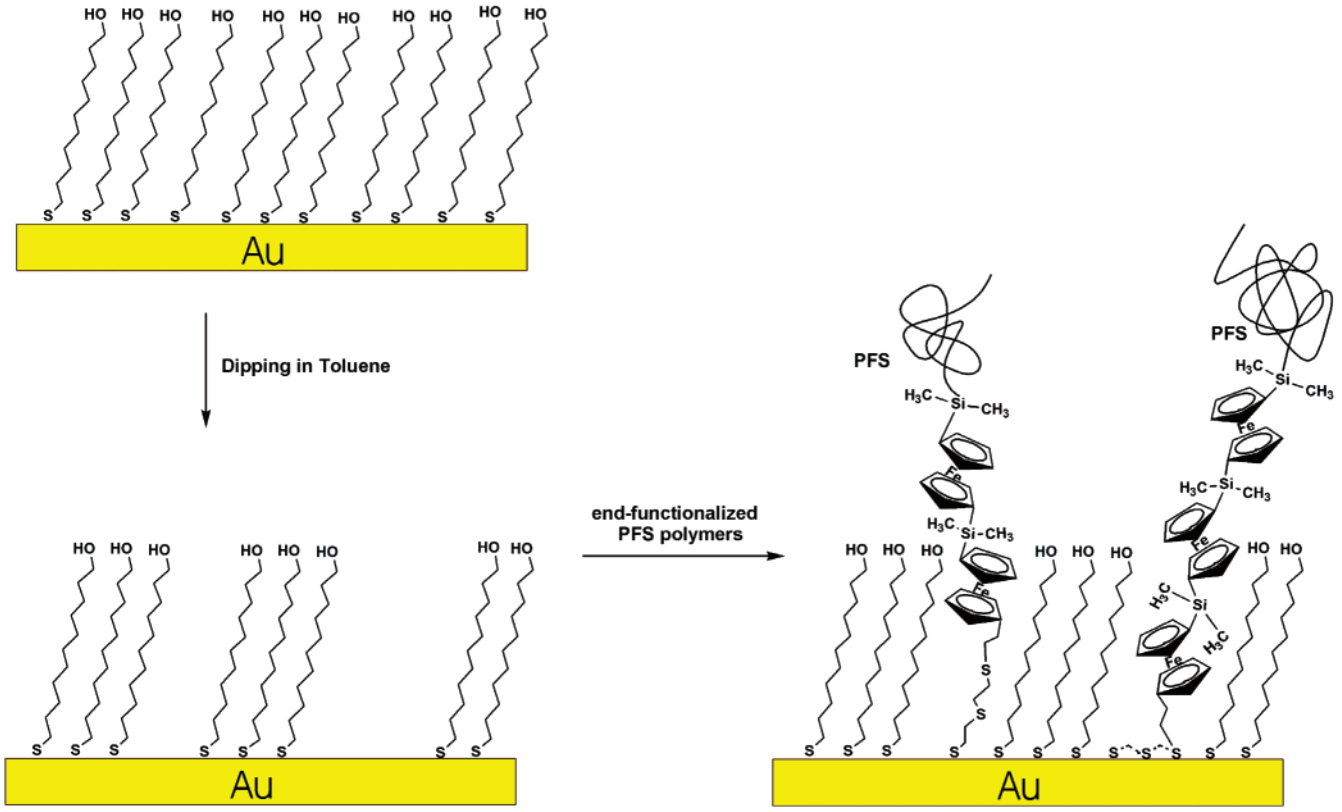

[a] Defects are created in SAMs of a mercaptoalkanol on gold by the in situ exposure to toluene. Ethylene sulfide end-functionalized PFS inserts into these defects and is covalently bound to the gold via its mercapto end group

Experimental Section

Materials. Ethylene sulfide end-functionalized poly(ferrocenyldimethylsilanes), prepared by treating living poly(ferrocenyldimethylsilanes) with ethylene sulfide, were available from previous studies.[22] The notation of the polymers corresponds to the monomer/initiator ratios. The following molar mass data were determined by GPC in THF, relative to polystyrene standards: PFS_{50} (M_n = 12 500 g/mol, DP_n = 50, M_w/M_n = 1.14), PFS_{100} (M_n = 22 600 g/mol, DP_n = 92, M_w/M_n = 1.13). 11-Mercapto-1-undecanol and 2-mercaptoethanol were purchased from Aldrich Chemical Co., and 6-mercapto-1-hexanol was purchased from Fluka Chemical Co. and used as received.

Substrates and Samples. (a) Gold substrates (11 mm × 11 mm, 250 nm Au on 2 nm Cr on borosilicate glass) for AFM measurements were purchased from Metallhandel Schröer GmbH (Lienen, Germany). Au(111) samples were obtained by annealing these substrates in a high-purity H_2 flame for 5 min.[31] (b) Round gold substrates for electrochemistry measurements (2.5 cm diameter, 200 nm gold on 5 nm Ti primer deposited onto glass substrates in a vacuum of 5×10^{-6} mbar) were purchased from SSENS bv (Hengelo, The Netherlands). Prior to use, these substrates were cleaned in Piranha solution (7:3 H_2SO_4/H_2O_2 (30%) by volume) and then rinsed with Milli-Q water and ethanol and dried in a nitrogen stream. ***Caution: Piranha solution should be handled with extreme caution; it has been reported to detonate unexpectedly.***

Self-assembled monolayers (SAMs) of 2-mercaptoethanol (C2OH), 6-mercapto-1-hexanol (C6OH), and 11-mercapto-1-undecanol (C11OH) were prepared by immersing cleaned gold substrates into 0.5×10^{-3} M solutions in ethanol overnight to ensure maximum coverage and order. For the investigation of mixed surface layers, insertions were carried out by dipping rinsed (dichloromethane, ethanol, MilliQ water, ethanol, and dichloromethane in sequence) substrates with preformed SAMs into solutions of PFS of the corresponding DP and concentration for different times (see text for details). For the single PFS_{100} chain stretching experiments, samples were prepared by immersion in 0.5×10^{-3} M 11-mercapto-1-undecanol overnight, followed by rinsing and dipping into a 8×10^{-6} M PFS in toluene solution (standard solution) for 2 min. After they were dipped into the PFS solutions, the samples were cleaned by placing them in toluene (20 mL) and dichloromethane (20 mL) for 10 min, respectively, followed by drying in a stream of nitrogen. The PFS solutions were deaerated with argon gas and covered with aluminum foil to prevent oxidation. All the pieces of glassware used were cleaned with Piranha solution and subsequently rinsed with large amounts of MilliQ water.

Cyclic Voltammetry (CV) and Differential Pulse Voltammetry (DPV) Experiments. Measurements were performed using an Autolab PGSTAT10 potentiostat (ECOCHEMIE, Utrecht, The Netherlands) in a three-electrode configuration. The gold substrate covered with the corresponding layer was used as the working electrode, $Hg/HgSO_4$ (MSE) was used as reference (+0.61 V_{NHE}), and Pt wire was used as the auxiliary electrode. The electrolyte was 0.1 M aqueous $NaClO_4$. The working electrode exposed a surface area of 0.44 cm^2 to the electrolyte. Prior to the measurements, the cell was degassed by passing nitrogen through the electrolyte for 5 min. Cyclic voltammograms were recorded between −0.4 V_{MSE} and +0.4 V_{MSE} at different scan rates. Differential pulse voltammograms were recorded at a pulse amplitude of 10 mV, a pulse time of 50 ms, and a time interval of 200 ms.

Contact Angle Measurements. Contact angles were measured right after preparing the samples, with an OCA 15 plus (Dataphysics Instruments GmbH, Germany) contact angle microscope equipped with a CCD camera. Advancing contact angles were determined automatically by drop shape analysis during the growth of the droplet at a constant flow rate (1 μL/s). Contact angles were measured using ultrasonically degassed MilliQ water.

(31) (a) Manne, S.; Butt, H.-J.; Gould, S. A. C.; Hansma, P. K. *Appl. Phys. Lett.* **1990**, *56*, 1758. (b) Schönherr, H.; Vancso, G. J.; Huisman, B.-H.; van Veggel, F. C. J. M.; Reinhoudt, D. N. *Langmuir* **1999**, *15*, 5541.

Atomic Force Microscopy (AFM) Measurements. Surface morphology measurements were carried out with a NanoScope IIIa atomic force microscope (Digital Instruments (DI), Santa Barbara, CA) equipped with a phase box. Tapping mode AFM scans were performed in air using silicon cantilevers/tips with a spring constant of 28−58 N/m (Nanosensors, Wetzlar, Germany). Force spectroscopy experiments were performed by in situ AFM in a liquid environment with a NanoScope IIIa multimode atomic force microscope fitted with a DI liquid cell (volume ~ 50 μL). Commercially available V-shaped Si_3N_4 cantilevers (DI) were used. Each cantilever was calibrated after a given experiment according to the equipartition method, by measuring the thermal excitation of the tip to compute its spring constant.[32] The measured spring constants of the cantilevers varied between 0.065 and 0.090 N/m. The number of nanometer-scaled features was determined by counting the features on at least three areas (each with a dimension of 300 × 300 nm^2) of the same sample and calculating the average.

Results

The insertion process of ethylene sulfide end-capped PFS into SAMs of ω-mercaptoalkanols on Au(111) was studied in detail in order to identify the parameters that control surface coverage. We investigated the effect of the insertion time, concentration of PFS solutions, and molar mass of PFS and the influence of the chain lengths of the thiol molecules. The effects of these parameters on the surface morphology, wettability, and polymer chain coverage were studied by means of AFM, contact angle, as well as cyclic and differential pulse voltammetry measurements. From this information the optimal conditions for preparing surfaces with low PFS coverages, preferably with individually isolated PFS macromolecules, are obtained for the targeted single PFS polymer chain stretching measurements by AFM.

The effect of adsorption time on surface coverage was estimated in cyclic voltammetry (CV) measurements of preformed SAMs of C6OH that were exposed to a 8×10^{-5} M PFS_{50} toluene solution for insertion times between 1 and 10 min. Complementary wettability data were obtained by contact angle measurements. The cyclic voltammograms of PFS layers show two reversible redox peaks, which are associated with the different oxidation potentials of Fe atoms with oxidized or neutral neighboring Fe atoms in the main chain, due to intermetallic coupling. Since the PFS molecules in our system are electroactive, the surface coverage of ferrocenyl sites (Γ_{Fc}) for all layers can be determined according to eq 1[23b,33]

$$\Gamma_{Fc} = \frac{Q_{Fc}}{n_e F A} \qquad (1)$$

where Q_{Fc} is the charge passed for the oxidation/reduction of ferrocenyl sites, n_e is the number of electrons involved in the electron-transfer process (here $n_e = 1$), F is the Faraday constant (F = 96 485 C·mol^{-1}), and A is the geometric surface area of the electrode (A = 0.44 cm^2).

Γ_{Fc} is calculated by integrating the areas under the redox peaks of the cyclic voltammograms. Then the number of grafted chains per unit area (Γ) is calculated by dividing Γ_{Fc} by the degree of polymerization. The corresponding advancing contact angles and surface coverages, obtained by analyzing the cyclic voltammograms (see e.g. Figure 1) according to eq 1, are shown in Table 1.

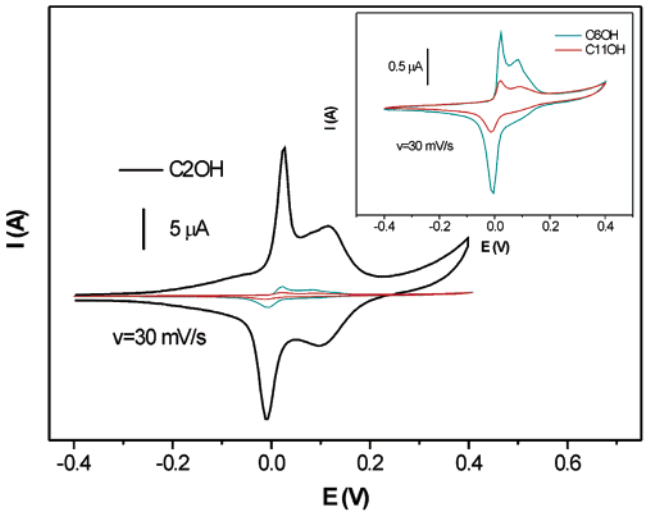

Figure 1. Cyclic voltammograms for PFS_{50} end-grafted from toluene (concentration: 8×10^{-5} M) into different SAMs for 2 min: C2OH, C6OH, and C11OH (scan rate v = 30 mV/s, 0.1 M $NaClO_4$ aqueous electrolyte, reference electrode $Hg/HgSO_4$, counter electrode Pt). The inset shows the data for PFS inserted into C6OH and C11OH with an enlarged ordinate.

Table 1. Advancing Contact Angles, Values of Charge, and Surface Coverages for Insertion of PFS_{50} from Toluene (Concentration: 8×10^{-5} M) into 6-Mercapto-1-hexanol Monolayers (C6OH) for Different Time Intervals

t (min)	1	2	4	10
θ_a (deg)	51 ± 2	51 ± 2	51 ± 2	51 ± 2
$10^6 Q_{Fc}$ (C)	2.0 ± 0.5	2.6 ± 0.5	1.8± 0.5	2.7 ± 0.5
$10^3\Gamma$ (chain/nm^2)	5.7 ± 0.1	7.4 ± 0.1	5.1 ± 0.1	7.7 ± 0.1

Table 2. Advancing Contact Angles, Values of Charge, and Surface Coverage for Insertion of PFS_{50} from Toluene (Concentration: 8×10^{-6} M) into C2OH, C6OH, and C11OH, Respectively, for 2 min Compared with Values of a PFS_{50} Full Layer

	θ_a (deg)	Q_{Fc} (C)	Γ (chain/nm^2)
full coverage	96 ± 2	(1.00 ± 0.05) × 10^{-4}	(2.80 ± 0.06) × 10^{-1}
C2OH	86 ± 2	(1.10 ± 0.07) × 10^{-5}	(3.10 ± 0.19) × 10^{-2}
C6OH	27 ± 2	(4.30 ± 0.21) × 10^{-7}	(1.20 ± 0.06) × 10^{-3}
C11OH	21 ± 2	(2.20 ± 0.11) × 10^{-7}	(6.20 ± 0.31) × 10^{-4}

The advancing contact angles for each insertion time are identical to within the experimental error; thus, all these samples exhibit equal surface hydrophobicity averaged over the contact area with the water drop used in the contact angle experiments. The PFS_{50} surface coverages for different insertion times also showed no significant difference. These data indicate that the insertion process has reached its dynamic equilibrium within even the shortest accessible experimental time interval. On the basis of this conclusion, we fixed a standard time of 2 min for all other experiments.

The effect of chain lengths of the thiol molecules, concentration of PFS solutions, and molar masses of PFS on polymer surface coverage was investigated in detail by electrochemistry. SAMs of C2OH, C6OH, and C11OH on gold were exposed to PFS_{50} solutions in toluene for 2 min. Drastically different coverages were observed by CV (Figure 1). The PFS surface coverage decreases markedly with increasing length of the alkane segment of the mercaptoalkanols comprising the SAMs; at the same time the values of the contact angles are lower. Values of quantitative surface coverages estimated from the CV data using eq 1 and the corresponding advancing contact angles are summarized in Table 2.

(32) (a) Florin, E. L.; Rief, M.; Lehmann, H.; Ludwig, M.; Dornmair, C.; Moy, V. T.; Gaub, H. E. *Biosens. Bioelectron.* **1995**, *10*, 895. (b) Butt, H. J.; Jaschke, M. *Nanotechnology* **1995**, *6*, 1.

(33) Forster, R. J.; Keyes, T. E.; Vos, J. G. *Interfacial Supramolecular Assemblies*; John Wiley & Sons Ltd: Chichester, England, 2003; Chapter 3, p 65.

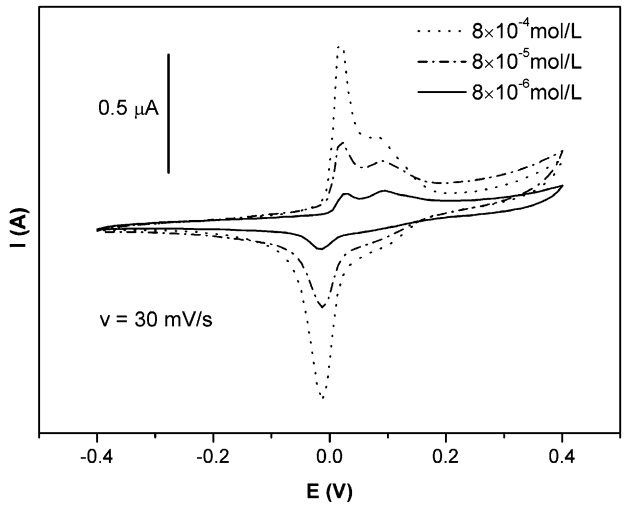

Figure 2. Cyclic voltammograms of samples obtained by insertion of PFS_{50} from 8×10^{-4} M, 8×10^{-5} M, and 8×10^{-6} M toluene solution into C11OH (scan rate $v = 30$ mV/s, 0.1 M $NaClO_4$ aqueous electrolyte, reference electrode $Hg/HgSO_4$, counter electrode Pt).

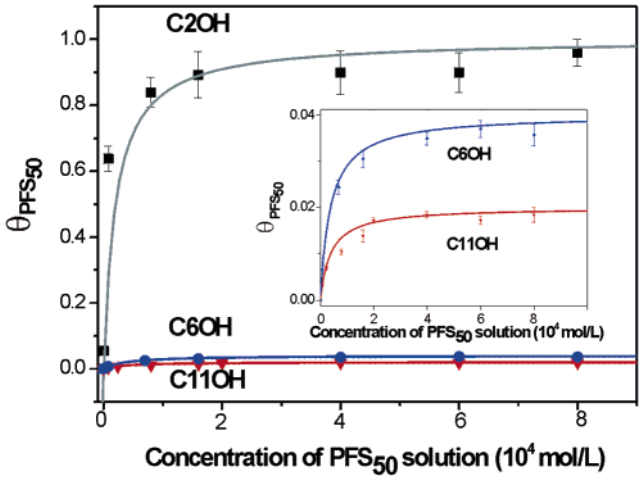

Figure 3. The dependence of PFS_{50} surface coverage normalized to the equilibrium coverage of C2OH determined by cyclic voltammetry on concentration of PFS_{50} for insertion into (A) C2OH, (B) C6OH, and (C) C11OH. The inset shows the data for C6OH and C11OH in more detail. The lines correspond to fitted Langmuir isotherms.

An increase in concentration of the PFS_{50} solution used for insertion led to similar changes obtained for a decrease in chain lengths of the thiol molecules. Advancing contact angles measured with water on samples prepared by insertion of PFS_{50} into C2OH, C6OH, and C11OH increased with increasing PFS concentration (see Supporting Information, Figure S1). A similar trend was observed in detailed CV experiments. Figure 2 shows the comparison of cyclic voltammograms of samples obtained by insertion of PFS_{50} from 8×10^{-4}, 8×10^{-5}, and 8×10^{-6} M toluene solution into C11OH for 2 min. The peak currents (i_{pc} and i_{pa}), as well as the charge transfer in the redox process, increased with increasing concentration.

The coverage data obtained for all SAMs can be fitted with a Langmuir isotherm (eq 2),[34] assuming that the maximum surface coverage (θ) in each set is equal to $\theta = 1.0$.

$$\theta = \frac{kc}{1 + kc} \qquad (2)$$

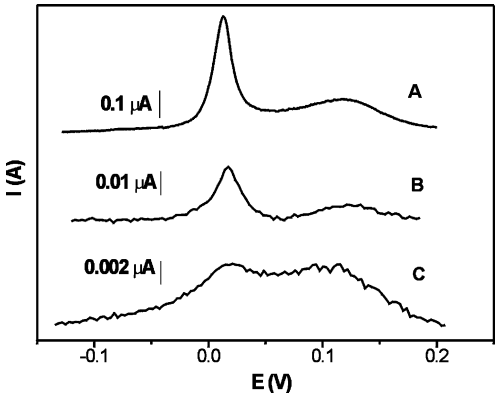

Figure 4. Differential pulse voltammograms recorded on PFS_{50} end-grafted from (A) 8×10^{-6} M, (B) 8×10^{-7} M, and (C) 2×10^{-7} M toluene solution into C11OH (pulse time 50 ms, interval time 200 ms, pulse height 10 mV, 0.1 M $NaClO_4$ aqueous solution).

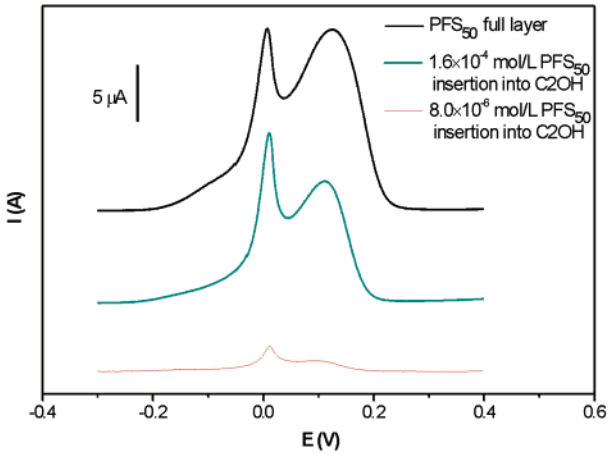

Figure 5. Differential pulse voltammograms recorded on a full layer of PFS_{50}, PFS_{50} inserted from 1.6×10^{-4} M toluene solution into C2OH, and PFS_{50} inserted from 8×10^{-6} M toluene solution into C2OH.

θ is the relative PFS surface coverage; c is the concentration of the PFS solution, and k is the equilibrium constant.

The fitted data are shown in Figure 3. It is observed that the k values obtained, which denote the ratio between the adsorption and desorption rate constants, decrease from 5.0×10^{-4} L/mol to 2.6×10^{-4} L/mol and 1.7×10^{-4} L/mol for C2OH, C6OH, and C11OH, respectively, showing that the driving force for the adsorption process decreases with increasing chain length. These results agree well with the mentioned contact angle data, as well as AFM images (vide infra).

The effect of molar mass of the polymer on the adsorption process was investigated using PFS_{100}. CV measurements of samples prepared by insertion of PFS_{100} into C11OH from 4×10^{-6} M solution were carried out under exactly the same conditions as those for PFS_{50}, including identical monomer concentration. The CV data for both samples showed two reversible redox peaks, and the integrated charge transfer values ($\sim 2.2 \times 10^{-7}$ C) in these two voltammograms are the same (see Supporting Information, Figure S2). Thus, the molar masses of the polymer molecules have no pronounced effect on the obtained surface coverages.

Since the detection limit of CV ($\sim 10^{-7}$ A) limits the quantification of surface coverage to $\sim 10^{-5}$ chain/nm^2,

(34) Atkins, P. W. *Physical Chemistry*, 6th ed.; Oxford University Press: Oxford, Melbourne, Tokyo, 1998; Chapter 28.

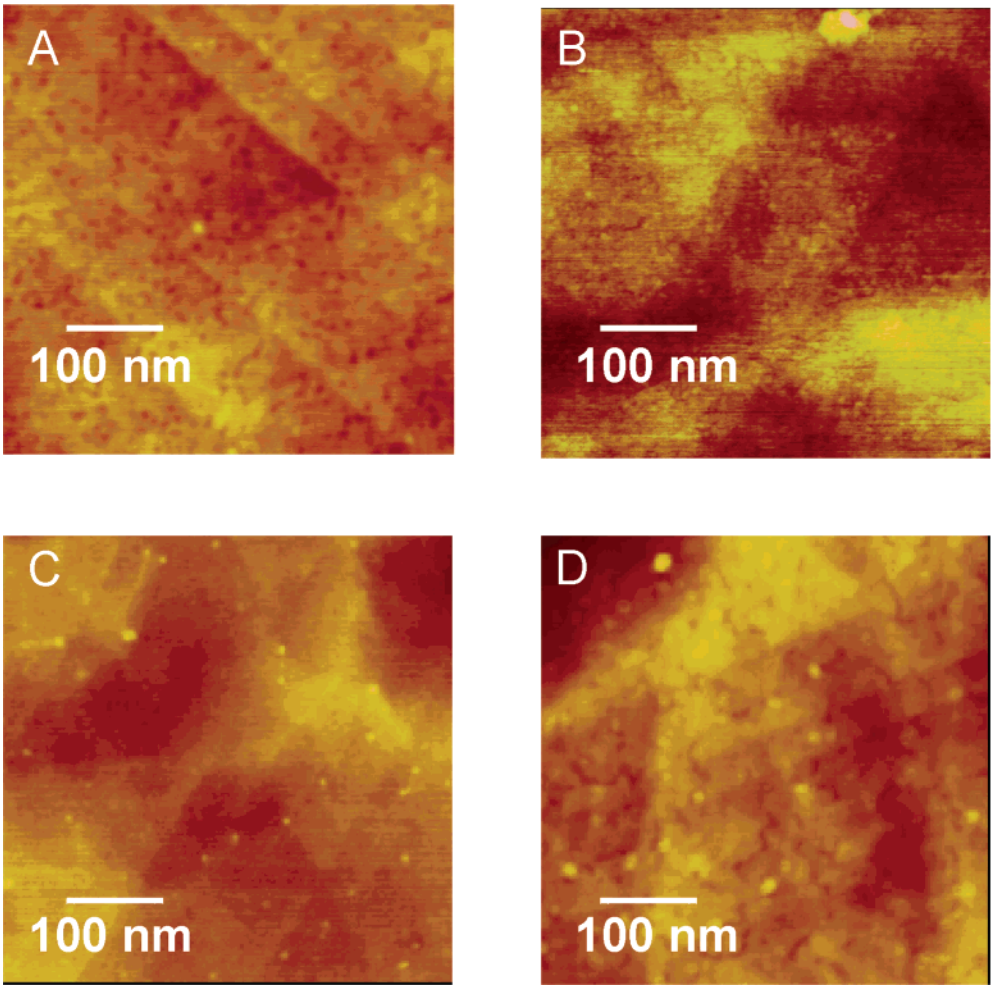

Figure 6. TM-AFM height images (acquired in air) for (A) a bare SAM of C11OH on Au(111); and after insertion of PFS_{50} from toluene (concentration: 8×10^{-6} M) into (B) C2OH, (C) C6OH, and (D) C11OH on Au(111) for 2 min (scan size 500 nm × 500 nm, *z* range is 10 nm for all images). The rms roughness of the neat SAM shown in part A of 0.2 nm increases to 0.5 nm after assembly of a full layer of PFS_{50} (B).

further investigations on the very low coverage PFS layers were based on differential pulse voltammetry (DPV) and the Langmuir isotherms (Figure 3) to predict the value of the surface coverage. Figure 4 shows the differential pulse voltammograms measured on samples prepared by insertion of PFS from different concentrations of PFS_{50} solutions into C11OH.

The two oxidation peaks can still be clearly resolved in the differential pulse voltammogram, although the CV (no data shown) did not show any oxidation waves on the samples shown in Figure 4B and C. The coverages calculated according to the Langmuir isotherm were $\Gamma \sim 5 \times 10^{-5}$ chain/nm^2 for PFS insertion from 8×10^{-7} M (B) and $\Gamma \sim 1 \times 10^{-5}$ chain/nm^2 for PFS insertion from 2×10^{-7} M solution (C). The detection limit for DPV was estimated as $\Gamma \sim 10^{-6}$ chain/nm^2, which is obtained by insertion of PFS from 1×10^{-7} M solution into C11OH.

For the ultimately targeted single molecule force spectroscopy experiments of surface-immobilized PFS, isolation of the chains is required. As seen in DPV experiments, the properties of PFS chains inserted into SAMs on gold showed an apparent difference compared to those in neat PFS layers. Figure 5 compares the DPV results for a full layer of PFS_{50} with those for PFS_{50} isolated with high and low coverages in a C2OH SAM.

In the voltammograms shown in Figure 5, the integral of the first peak (seen as a shoulder at −0.1 V), which is attributed to the oxidation of the small fraction of Fe atoms that are in close proximity to the gold surface,[19d,23b,35] is decreasing relative to that of the second peak with decreasing PFS coverage. Furthermore, the ratio of the integrated areas under the second and third oxidation peaks changed gradually from 1:2 to 1:1. The same effects were also observed for PFS_{100} (see Supporting Information, Figure S3). After insertion of PFS into SAMs, the first oxidation peak virtually disappeared and the integrated area under the remaining two peaks changed to 1:1.

These CV and CA results were complemented by tapping mode AFM data acquired in air (Figure 6). All images present triangular terraces with 60° angles, which are typical for Au(111).[31] Figure 6A shows a bare SAM, which appears to be homogeneous, except for the well-known depressions in the gold,[36] while for PFS inserted into SAMs, densely packed, barely protruding (Figure 6B) and isolated elevated, round (Figure 6C and D) features were revealed. These round features have an average height of 4 ± 2 nm and an average diameter of 10−12 nm, as estimated in cross-sectional analyses. As the thiol chain length changes from C2 to C11, less features are observed (vide infra). The same trend was detected for decreasing concentrations (see Supporting Information, Figure S4).

If we assume the specific gravity (ρ) of the PFS_{50} polymer to be the same as the bulk value of PFS (1.26 g/cm^3)[23c] and

(35) Rulkens, R.; Lough, A. J.; Manners, I.; Lovelace, S. R.; Grant, C.; Geiger, W. E. *J. Am. Chem. Soc.* **1996**, *118*, 12683.
(36) Poirier, G. E. *Langmuir* **1997**, *13*, 2019 and references therein.

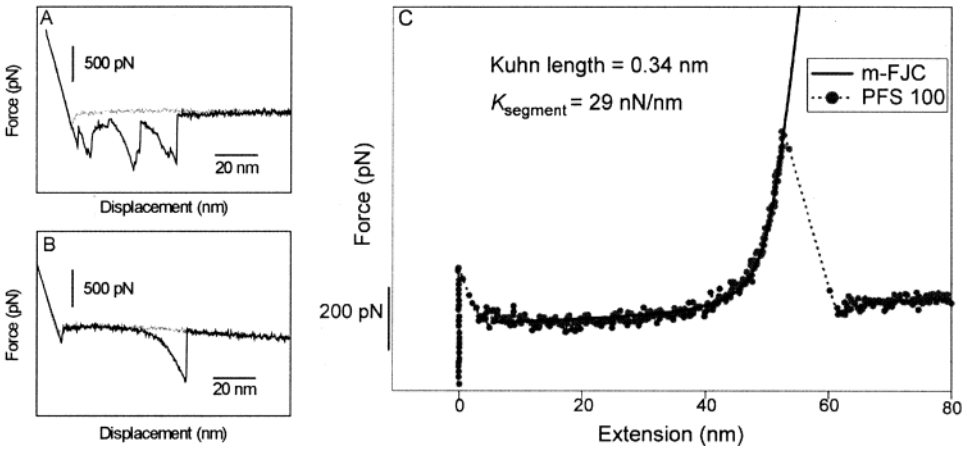

Figure 7. Representative force-displacement curves obtained by in situ AFM using isopropanol as the solvent on (A) a PFS_{100} full layer and (B) isolated PFS_{100} macromolecules inserted from 8×10^{-6} M toluene solution into C11OH (AFM cantilever spring constant: 0.08 ± 0.015 N/m). (C) Measured force curve of the PFS_{100} polymer chain and superimposed fit using the modified FJC model.[38] The fit parameters for this particular force extension curve are shown.

Table 3. Amount of Charge and Surface Coverage Data by CV and TM-AFM, Respectively, for PFS_{50} Inserted into C6OH and C11OH from Toluene for 2 min

		Γ (chain/nm^2)	
SAM	Q_{Fc} (C)	by CV	by AFM
C6OH	$(4.3 \pm 0.2) \times 10^{-7}$ [a]	$(1.2 \pm 0.1) \times 10^{-3}$	$(3.0 \pm 0.9) \times 10^{-4}$
C11OH	$(2.2 \pm 0.1) \times 10^{-7}$ [a]	$(6.2 \pm 0.3) \times 10^{-4}$	$(4.2 \pm 0.2) \times 10^{-4}$
C11OH	$(1.6 \pm 0.1) \times 10^{-6}$ [b]	$(4.5 \pm 0.4) \times 10^{-3}$	$(5.5 \pm 0.4) \times 10^{-3}$

[a] Concentration: 8×10^{-6} M. [b] Concentration: 8×10^{-4} M.

the molecular mass (M_n) of PFS_{50} as 12 500 g/mol, the average volume that one PFS_{50} molecule occupies is calculated to be 17 nm^3 by using the following equation:

$$\bar{V}_i = \frac{M_n}{N_A \rho} \tag{3}$$

where N_A is the Avogadro constant ($N_A = 6.022 \times 10^{23}$ mol^{-1}). The diameter of a sphere that corresponds to this volume value is 3.2 nm, which is calculated by

$$D = 2\left(\frac{3\bar{V}_i}{4\pi}\right)^{1/3} \tag{4}$$

Considering that the polydispersity of the PFS_{50} polymer chains in our experiment is 1.14,[23] the theoretical diameter of a spherical polymer chain will have an approximate value of ~2−4 nm. The height of the observed features (4 ± 2 nm) is in excellent agreement with this value, thus indicating the dotlike features observed in the TM-AFM images above are single PFS_{50} polymer chains. For PFS_{50} insertion into C6OH and C11OH, the surface coverages of PFS_{50} on gold (Figure 6C and D) were determined by counting the number of features in areas of 300×300 nm^2. The corresponding result was compared with the surface coverages obtained from the CV measurements, as shown in Table 3. Especially for the long-chain SAM (smaller relative error), the agreement of the surface coverage values obtained by the different techniques is very good.

Finally, the elasticity of PFS_{100} polymer chains in neat layers and as *isolated* chains was probed by single molecule force spectroscopy (SMFS). These experiments were carried out by in situ AFM using ethanol and isopropanol as the solvent and normal Si_3N_4 cantilevers. Figure 7A shows the force−displacement curve acquired in SMFS experiments on neat layers of PFS_{100} on Au. Multiple force signals are present in the plot. By contrast, the force−displacement curves of stretched PFS chains that are immobilized as isolated chains on the sample show single stretching and pull-off events, as illustrated in Figure 7B.[37] The force-extension curves were fitted by the modified freely jointed chain (m-FJC) (Figure 7C) and yielded a Kuhn length of 0.33 ± 0.05 nm and a segment elasticity $K_{segment}$ of 32 ± 5 nN/nm.[38] In the experiments on samples with isolated PFS chains, we obtained stretching events in less than 30% of the tip−sample contact cycles. The observed stretching events are similar to those detected in ethanol. The extension distance, representing the elastic response of the polymer (see Figure 7B), was about 55 nm.

(37) The frequency of observed stretching events was estimated as 1−2% for samples in which isolated PFS_{100} macromolecules were inserted from 8×10^{-6} M toluene solution into C11OH. While multiple force signals were frequently observed in neat SAMs, the frequency was <5% (on the basis of all successful stretching events) for samples exposing very few chains. Since multiple events are due to not only the multiple chain stretching but also stretching of multiple loops of a single chain, the data are most consistent with the notion that isolated chains are exposed on the corresponding samples.

(38) The m-FJC model (eq 5), which is typically used as a statistical model to describe the elongation of single polymer chains to large deformations, is an extension of the freely jointed chain (FJC) model.[16a,e,17] This simple FJC model can capture the entropic elasticity of polymer chains (for modest extensions) and describes the polymer as a chain of n rigid segments of equal length I_K without any long-range interactions. Before chemical bonds break, the deformation of bond angles and the stretching of covalent bonds will result in an effective increase in the segment length. Thus, enthalpic contributions to the restoring force of the polymer chain must be considered. As introduced by Smith et al. (Smith, S. B.; Cui, Y. J.; Bustamante, C. *Science* **1996**, *271*, 795.) in the m-FJC model, the extensibility of the segments can be considered as an additional Hookean term. The enthalpy elasticity is hence accounted for by modeling the molecule as n identical elastic springs with segment elasticity $K_{segment}$ in series.

$$x(F) = \left[\coth\left(\frac{FI_K}{k_B T}\right) - \frac{k_B T}{FI_K}\right]\left(L_{contour} + \frac{nF}{K_{segment}}\right) \tag{5}$$

where x is the extension of the polymer chain; F is the applied force; I_K (Kuhn length) is the length of the statistically independent segment; n is the number of segments, which equals $L_{contour}/I_K$; $K_{segment}$ is the segment elasticity, which characterizes the deformability of the segment; k_B is the Boltzmann constant; and T is the temperature. We note that the segment elasticity $K_{segment}$ is the elasticity of *one* segment; the elasticity of the whole polymer chain hence also depends on the degree of polymerization (number of segments n). In a recently published independent study, Shi et al. have reported single chain elasticity data for PFS: Shi, W.; Cui, S.; Wang, C.; Wang, L.; Zhang, X.; Wang, X.; Wang, L. *Macromolecules* **2004**, *37*, 1839.

Discussion

The systematic investigation of the insertion behavior of ethylene sulfide end-functionalized PFS derivatives into preformed SAMs was carried out in order to develop a robust and reproducible procedure that allows us to obtain individually isolated PFS macromolecules covalently attached to solid substrates for AFM-based single molecule force spectroscopy experiments. Upon exposure of SAMs of different ω-mercaptoalkanols on Au(111) to ethylene sulfide end-functionalized PFS, as shown above, layers with altered surface properties were obtained. On the basis of atomic force microscopy, contact angle, and electrochemistry measurements, the polymer surface coverage was shown to be sensitive to the chain length of the ω-mercaptoalkanols molecules and to the concentration of the PFS solution but not to the insertion time or to the molar mass of PFS.

The insensitivity to adsorption time on the time scales probed is likely related to the rapid defect formation and insertion of PFS into these defects. A corresponding replacement reaction would yield the same result. In a previous study it has been shown that the rate of defect formation is not the rate-limiting step.[29b] Since the molar mass of the ethylene sulfide end-functionalized PFS was not found to play a significant role in the attained coverages, the insertion process is unlikely diffusion controlled.

The surface hydrophilicity assessed by contact angle measurements decreased notably with decreasing chain length of the alkanethiols, as well as with increasing PFS concentration (Figure S1, Table 2). The electrochemistry (Figures 1−4, Table 2) and AFM data (Figures 6 and S4) showed the same trend. While the properties probed are very different for each of the three methods, the data are very consistent.

All preformed SAMs investigated present high-surface energy surfaces due to the exposed array of hydroxyl groups.[39] The advancing contact angles of ∼15−18°, which are in excellent agreement with the literature,[39] were found to increase after insertion of the more hydrophobic PFS chains (θ_a(PFS) = 96°). Since the contact angles of two component ultrathin films correspond to a weighted mean of the contact angles of the pure components,[40] the increase in hydrophobicity with both decreasing chain length and increasing concentration qualitatively indicates an increasing fraction of adsorbed PFS. However, the cross-sectional area of a thiol molecule and that of a PFS polymer coil are not identical; hence, the Cassie equation is not applicable to estimate the surface coverage quantitatively.

Cyclic voltammetry, on the other hand, can be employed in a quantitative manner to estimate the polymer surface coverage. The CV data fully confirmed the trends observed already in the wettability data. When the chain length in the preformed SAMs is increased from C2 to C11, the surface coverage values of PFS are dramatically reduced (Figure 1, Table 2). Compared to the neat layers of PFS, we observe a coverage which is 1, 2, or 3 orders of magnitude lower for PFS inserted into C2OH, C6OH, or C11OH, respectively. Similarly, the reduction in concentration of the PFS solutions leads to a decrease in surface coverage (Figures 2−4). Since the surface coverage can be successfully described by a Langmuir isotherm, the surface coverage at very low concentrations can be predicted. Direct proof for the presence of PFS in such layers and a qualitative dependence of coverage on concentration was obtained by DPV (Figure 4).

Furthermore, we observed an excellent agreement of the PFS_{50} surface coverages obtained by CV and those estimated from AFM images of samples prepared under exactly the same conditions (Figures 6 and S4). From the analysis of the AFM data (vide supra) and a comparison with the surface coverages obtained by CV, we conclude a good agreement of the number of elevated dotlike features observed by AFM and the number of PFS macromolecules deduced from the charge passed for oxidation and reduction (Table 3). This good agreement is a reliable confirmation for the interpretation that the isolated round features observed by AFM are indeed individual PFS macromolecules.

The exact dimensions of the surface-immobilized PFS macromolecules cannot be directly extracted from the AFM data. The corresponding feature heights (4 ± 2 nm) and diameters (10−12 nm) obtained from cross-sectional analyses may possess significant systematic errors. In particular, the width is certainly an overestimate due to tip convolution effects. Close inspection of Figure 6C and D reveals apparently different features sizes. These are caused by different tips utilized in the experiments. While a quantitative deconvolution is in principle possible, we have not deconvoluted the data, to avoid artifacts caused by such procedures. The feature height may appear too low due to compression of the polymer chain by the repulsive forces exerted by the AFM tip[41] or shifts of the resonance frequency due to adhesive interactions.[42,43] An apparent increase in height due to pronounced damping by the PFS chain cannot be ruled out a priori either.[44] However, we note that, under the conditions employed, these effects are likely to be smaller than the standard deviation estimated. In addition to the nanometer scale dimensions of the features observed in AFM images, the good agreement of surface coverages according to AFM and CV (Table 3) and the reduced interchain segment−segment interaction observed in DPV (vide infra) support our interpretation that the observed features are individual PFS macromolecules. The typical spacing of neighboring individual PFS chains of ≥40 nm (e.g. Figure 6) compared to the tip−sample contact area of approximately 1.7 nm^2 (ref 45) shows that multiple chain stretching in the SMFS experiments is very unlikely.

The control over the PFS surface coverage can be linked to the determinant role of PFS concentration for the driving force for adsorption on one hand and the mechanism of insertion, as well as the order and arrangement of the preformed SAMs, on the other hand. The concentration dependences, which can be described by Langmuir isotherms (Figure 3), are qualitatively similar for the three SAM systems described. The difference among the rate constants for adsorption and desorption for SAMs with different chain lengths is related to the structure and order of the corresponding SAM.

(39) Bain, C. D.; Evall, J.; Whitesides, G. M. *J. Am. Chem. Soc.* **1989**, *111*, 7155.

(40) Cassie, A. B. D. *Discuss. Faraday Soc.* **1948**, *3*, 11.

(41) Marsh, T. C.; Vesenka, J.; Henderson, E. *Nucleic Acids Res.* **1995**, *23*, 696.

(42) Van Noort, S. J. T.; Van der Werf, K. O.; De Grooth, B. G.; Van Hulst, N. F.; Greve, J. *Ultramicroscopy* **1997**, *69*, 117.

(43) Ebenstein, Y.; Nahum, E.; Banin, U. *Nano Lett.* **2002**, *2*, 945.

(44) Schönherr, H.; Frank, C. W. *Macromolecules* **2003**, *36*, 1199.

(45) Using Hertz theory (see e.g.: Nelles, G.; Schönherr, H.; Jaschke, M.; Wolf, H.; Schaub, M.; Küther, J.; Tremel, W.; Bamberg, E.; Ringsdorf, H.; Butt, H.-J. *Langmuir* **1998**, *14*, 808) and assuming a typical tip radius R of 25 nm, a reduced elastic modulus K of the contact of 64 GPa (see e.g.: Noy, A.; Frisbie, C. D.; Rozsnyai, L. F.; Wrighton, M. S.; Lieber, C. M. *J. Am. Chem. Soc.* **1995**, *117*, 7943), and a load of 1 nN, we obtain the radius of the contact area a as $a = [(R/K)L]^{1/3}$ (eq 6).

As shown previously, the rapid desorption of surface bound thiols as disulfides leads to the formation of defects in SAMs. Into these defects thiol or sulfide adsorbates insert and can subsequently covalently bind to the surface.[29] It is well established that the number of inherent defects, as well as the conformational irregularity of the monolayers, decreases with increasing chain length of the thiol adsorbates.[30] Owing also to the importance of interchain van der Waals interactions for SAM stability, an increase in chain length can be expected to result in a decrease in the number of new defects formed in the SAM, when it is exposed to toluene (Scheme 1). Thus, longer chain SAMs can be expected to possess fewer defects for insertion of end-functionalized PFS. In addition, it may also be argued that, depending on the size of the defect, there is an increasing difficulty of the thiol end group of the PFS to reach the gold surface for SAMs with increasing chain length. Consequently, the resulting PFS surface coverages should decrease with increasing chain length of the thiols comprising the SAMs.

In the absence of clustering, this low coverage implies the likely presence of isolated PFS chains. In particular, the DPV data show evidence in support of this assertion. The contribution of the small fraction of Fe atoms that are in close proximity to the gold surface to the oxidation trace of the differential pulse voltammograms (shoulder at −0.1 V) decreased with decreasing surface coverage (Figures 5 and S3). The reason might be that the number of Fe atoms that are closest to the gold surface becomes smaller with decreasing surface coverage of PFS on gold. In addition, the regularity of SAMs increases according to the increase of chain length of the thiol molecules.[30] Thus, the inert effect of long-chain SAMs on charge transfer results in a progressive difficulty for the Fe atoms to reach the gold surface. As shown in the voltammograms in Figures 5 and S3, the first peak becomes gradually undetectable.

More importantly, the ratio of the integrated areas under the second and third oxidation peaks changed from 1:2 to 1:1 (Figures 5 and S3). This observation is in good accordance with our previous results obtained on neat PFS layers.[23b] It has been argued that under poor solvent conditions the 1:2 ratio results from the consideration of the interchain segment−segment interactions between the polymer chains in the thin film. The 1:1 ratio indicates that most of the interchain segment−segment interactions among the PFS polymer chains are absent. As we already know from the CV measurements that in our procedure the PFS surface coverages were continuously decreasing, we conclude that the decreasing interchain PFS segment−segment interactions become negligible with decreasing PFS surface coverage.

These data indicate, together with the above-mentioned wettability, CV, and AFM data, that the surface-immobilized PFS macromolecules are indeed isolated as individual molecules. The force−displacement data recorded in AFM-based single molecule force spectroscopy measurements in different solvents on PFS_{100} are also fully consistent with this interpretation. While we observed multiple force signals (stretching and pull-off events) during the same retraction of the AFM tip from a neat PFS layer (Figure 7A), the same experiment carried out on isolated PFS chains led to the almost exclusive observation of single force signals (Figure 7B).

The multiple force signals observed for neat PFS layers are ascribed to multichain adsorption to the tip and subsequent simultaneous stretching.[15,16] In this case, the AFM tip adsorbs more than one chain and the chain that bears the highest load would detach first from the tip, followed by the other chains at a later stage. This scenario results in the multiple pull-off events observed. By contrast, the single events observed for experiments carried out on isolated PFS chains are an indication of the stretching of individual molecules.

Despite the different contour lengths of the polymers chains, all of the force−displacement curves acquired on isolated PFS chains show similar characteristics: the deflection rises monotonically with the extension of the polymer chain until a rupture point is reached; then the force drops suddenly to the origin state. The extension distance, representing the elastic response of the polymer (see Figure 7B), was in this case about 55 nm. This compared favorably with the contour length of the PFS_{100} polymer chain that can be estimated to be ∼58 nm by using the assumed mean length of the repeating unit as 6.3 Å[26a] multiplied by the degree of polymerization (92).

From the fit of the force−extension curves by the m-FJC model (Figure 7C) we can see that the extended Langevin function describes the elastic properties of PFS in both the low- and high-force regimes well.[16a,e] This indicates that the elasticity of PFS at low forces is dominated by the entropic contribution; in the high-force regime, the elasticity of PFS is governed by both entropy and enthalpy. By fitting more than 40 experimental force−extension curves of different contour lengths, we found that all of the PFS filaments possess an identical Kuhn length of 0.33 ± 0.05 nm and a segment elasticity $K_{segment}$ of 32 ± 5 nN/nm,[38] although the lengths of these filaments vary from 20 to ∼60 nm.

These two findings, the linear scaling of the elastic properties with the contour lengths and the identical segment elasticities and Kuhn lengths for all polymer chains, corroborate that individual PFS chains are stretched and the deformation of a *single* chain under tension is measured. Since PFS is end-grafted covalently onto gold surfaces and was stretched in isopropanol, the resultant PFS layer consists mainly of PFS loops and tails of various lengths. Thus, the deformation of single PFS filaments in this study represents the deformation of single PFS loops or tails.

As mentioned in the Introduction, surface-immobilized PFS has been shown previously to undergo reversible redox-induced morphology and volume/thickness changes in neat self-assembled layers on gold.[22,23] These effects, which are related to the changes in solubility and conformation of the macromolecules upon oxidation or reduction, respectively, can be expected to alter their elasticity as well. Thus, in conjunction with the immobilization strategy reported here, it is in principle possible to fabricate a true molecular machine based on this surface-immobilized stimulus-responsive PFS system.

Conclusions

PFS macromolecules were successfully immobilized on gold surfaces through the insertion of PFS into preformed self-assembled monolayers of hydroxyl-terminated alkanethiols on gold from toluene solution. AFM, contact angle, and electrochemical measurements were carried out to characterize the morphology, wettability, and surface coverages of the mixed layers. The data obtained complement each other and agree well with each other. PFS surface coverages depended on the chain length of the thiol molecule and the concentration of the PFS toluene solution but not the insertion time and the chain length of the end-functionalized PFS molecules. Very low surface coverages were achieved by using insertion from very dilute PFS solution into long-chain SAMs. Differential

pulse voltammetry provided a very useful tool in elucidating the isolation effects that exist in mixed layers of lower PFS surface coverage. In samples with very low PFS surface coverages most of the interchain interactions were avoided, which is a requirement for the investigation of single PFS chain behavior by single molecule force spectroscopy. The immobilized isolated PFS_{100} macromolecules were subjected to in situ AFM for SMFS measurements for the first time in ethanol and isopropanol. The elasticity of the PFS_{100} single polymer chain was revealed by fitting the experimental results with the m-FJC model, which showed entropic and partly enthalpic elastic behavior of this polymer in these media.

Acknowledgment. The authors acknowledge Dr. M. Péter and Dr. R. G. H. Lammertink for their contribution in the synthesis of PFS. This work has been financially supported by the Council for Chemical Sciences of The Netherlands Organization for Scientific Research (CW-NWO), the $MESA^+$ Institute for Nanotechnology of the University of Twente ($MESA^+$ SRO *Nanolink*), and the University of Twente (Faculty of Chemical Engineering and Delta National scholarship).

Supporting Information Available: Contact angle data for different concentrations, DPV data for different molar masses of PFS, DPV data for different surface coverages of PFS100, and AFM data of PFS50 for different concentrations.

LA036341I